

Article

High-Temperature Tribological Performance of Al₂O₃/a-C:H:Si Coating in Ambient Air

Vitali Podgursky ¹, Asad Alamgir ^{1,*}, Maxim Yashin ¹, Taivo Jõgiaas ², Mart Viljus ¹, Taavi Raadik ³, Mati Danilson ³, Fjodor Sergejev ¹, Andreas Lümekemann ⁴, Jan Kluson ⁵, Jozef Sondor ⁶ and Andrei Bogatov ¹

¹ Department of Mechanical and Industrial Engineering, Tallinn University of Technology, Ehitajate tee 5, 19086 Tallinn, Estonia; vitali.podgurski@taltech.ee (V.P.); maximyash92@gmail.com (M.Y.); mart.viljus@taltech.ee (M.V.); fjodor.sergejev@taltech.ee (F.S.); andrei.bogatov@mail.ru (A.B.)

² Institute of Physic, University of Tartu, W. Ostwaldi 1, 50411 Tartu, Estonia; taivo.jogiaas@ut.ee

³ Department of Materials and Environmental Technology, Tallinn University of Technology, Ehitajate tee 5, 19086 Tallinn, Estonia; taavi.raadik@taltech.ee (T.R.); mati.danilson@taltech.ee (M.D.)

⁴ PLATIT AG, Eichholzstrasse 9, 2545 Selzach, Switzerland; a.luemkemann@platit.com

⁵ PLATIT a.s., Prumyslova 3020/3, 787 01 Sumperk, Czech Republic; j.kluson@platit.com

⁶ LISS a.s., Coating Center PLATIT, Dopravní 2603, 756 61 Rožnov pod Radhoštěm, Czech Republic; j.sondor@liss.cz

* Correspondence: asad.shaikh@taltech.ee

Abstract: The study investigates thermal stability and high temperature tribological performance of a-C:H:Si diamond-like carbon (DLC) coating. A thin alumina layer was deposited on top of the a-C:H:Si coating to improve the tribological performance at high temperatures. The a-C:H:Si coating and alumina layer were prepared using plasma-activated chemical vapour deposition and atomic layer deposition, respectively. Raman and X-ray photoelectron spectroscopy were used to investigate the structures and chemical compositions of the specimens. The D and G Raman peaks due to sp² bonding and the peaks corresponding to the trans-polyacetylene (t-Pa) and sp bonded chains were identified in the Raman spectra of the a-C:H:Si coating. Ball-on-disc sliding tests were carried out at room temperature and 400 °C using Si₃N₄ balls as counter bodies. The a-C:H:Si coating failed catastrophically in sliding tests at 400 °C; however, a repeatable and reproducible regime of sliding with a low coefficient of friction was observed for the Al₂O₃/a-C:H:Si coating at the same temperature. The presence of the alumina layer and high stress and temperature caused structural changes in the bulk a-C:H:Si and top layers located near the contact area, leading to the modification of the contact conditions, delivering of extra oxygen into the contact area, reduction of hydrogen effusion, and suppression of the atmospheric oxidation.

Keywords: diamond-like carbon; alumina; thermal stability; adaptation; tribology; wear



Citation: Podgursky, V.; Alamgir, A.; Yashin, M.; Jõgiaas, T.; Viljus, M.; Raadik, T.; Danilson, M.; Sergejev, F.; Lümekemann, A.; Kluson, J.; et al. High-Temperature Tribological Performance of Al₂O₃/a-C:H:Si Coating in Ambient Air. *Coatings* **2021**, *11*, 495. <https://doi.org/10.3390/coatings11050495>

Academic Editor: Kevin Plucknett

Received: 1 April 2021

Accepted: 21 April 2021

Published: 23 April 2021

Publisher's Note: MDPI stays neutral with regard to jurisdictional claims in published maps and institutional affiliations.



Copyright: © 2021 by the authors. Licensee MDPI, Basel, Switzerland. This article is an open access article distributed under the terms and conditions of the Creative Commons Attribution (CC BY) license (<https://creativecommons.org/licenses/by/4.0/>).

1. Introduction

The minimisation of heat generation, friction, and wear demand in industry is an essential issue for sustainable development [1]. Carbon-based coatings have wide industrial applications (aerospace, automotive, machine tools, medical implants, etc. [1,2]) owing to their low coefficient of friction (COF) for different types of friction pairs, good mechanical properties, and chemical inertness. The challenge is that these properties should be retained during intensive use of such coatings under aggressive conditions (temperature, atmosphere, irradiation, etc.).

The tribological performance of carbon-based coatings is sensitive to their properties (hardness, internal stress, adhesion, thermal stability, oxidation resistance, surface roughness, etc.) and test conditions (sliding regimes, atmosphere, temperature, etc.). In addition to the preparation of carbon-based coatings using different deposition techniques, there are some straightforward approaches to modifying the structure of the coatings. First, the surface and bulk properties can be changed by doping, annealing, and irradiation.

Second, modification of the surface properties of the coating can be accomplished by using different lubricants and ambient environments, post-treatment of the surface by plasma, deposition of thin adaptive layers, etc. Third, the properties of the coating can be changed in situ in tribological tests owing to mechanochemical processes. The frictional heat dissipated within the coating and high stress within the contact area can cause changes in the coating structure.

The main components of the structure of diamond-like carbon (DLC) and tetrahedral amorphous carbon (ta-C) are the networks of sp^2 and sp^3 bonds and impurities (H, O, N, Si, Ti, W, etc.). Inclusions of sp -hybridised trans-polyacetylene (t-Pa) and poly(p-phenylene vinylene) chains were revealed in an a-C:H coating by resonant Raman scattering [3]. Longer and shorter t-Pa chains were found in DLC [4], and the formation of two types of sp -hybridised chains (cumulene and polyynes) were reported by Ravagnan et al. [5].

The sp^2 and sp^3 bonds play a key role in the unique mechanical and tribological properties of DLC and ta-C coatings. The crucial parameters are the sp^3 content, clustering and orientation of the sp^2 phase, cross-sectional nanostructures, and hydrogen content [6]. High internal stress occurs in DLC coatings because of the large fraction of highly tensile-strained sp^3 C–C bonds [7]. It is accepted that the sp^3 bond network affects the thermal stability and mechanical properties (hardness, Young's modulus) of DLC and ta-C coatings [6,8,9]. The configuration of the order/disorder within the sp^2 phase can also influence the mechanical properties [10]. At a relatively low temperature (200–300 °C), the graphitisation or transformation of sp^3 to sp^2 bonds occurs in DLC coatings [11–13]. Stress-induced graphitisation can also occur because of the high contact pressure in sliding tests [9]. High hardness, surface smoothness, and viscoelasticity/viscoplasticity are properties that strongly influence the tribological behaviour of DLC coatings [14–17]. The passivation of dangling bonds by different agents (H, hydroxyl (–OH), carboxyl (–COOH), etc.), graphitisation, and the formation of a self-generated easy-shearing transfer layer consisting of carbon-based structures, oxides, water, etc., are the main mechanisms explaining the excellent tribological properties of DLC and ta-C coatings, including superlubricity (COF < 0.01 [18]) [14,19–23]. Hydrogen and oxygen thus play important roles in understanding the friction mechanisms of DLC and ta-C coatings.

There is increasing interest in improving the thermal stability, oxidation resistance, and tribological properties of carbon-based materials under harsh conditions. One of the most successful approaches is doping the a-C:H coating with Si. Low internal stress, good adhesion [24], and enhanced thermal stability have been observed for a-C:H:Si coatings [25,26], and a high load-bearing capacity was demonstrated for a Si-doped DLC coating at room temperature (RT) [27]. The high temperature tribological properties of DLC and Si-doped DLC depends on numbers of factors, for instance, applied load, sliding distance, wear scar radius, counterbody material, etc. [24–26]. A significant fraction of C–Si bonds forms within the a-C:H matrix, which inhibits the formation of strained C–C bonds. This reduces the probability of sp^3 to sp^2 transformation, resulting in higher thermal stability [7]. Further improvements in the thermal stability and tribological properties have been achieved by doping a-C:H with both silicon and oxygen to form an a-C:H:Si:O structure [28–30]. It was reported in a seminal publication [29] that under low Earth orbit conditions, a-C:H:Si:O was more stable than an a-C:H coating. It was stressed that good tribological properties, thermal stability, and suppression of oxidation are caused by the formation of a SiO_2 layer on top of a-C:H:Si and a-C:H:Si:O, in contrast to the a-C:H coating. Oxygen preferentially bonds to silicon in the a-C:H:Si:O coating, forming small local amorphous clusters of a-Si:O [7]. An increase in the hardness and residual stress was observed for an oxygen-doped Si-free a-C:H:O coating, in contrast to the a-C:H coating [31].

Annealing and surface treatment with oxygen-containing gases are used to modify the properties of DLC, ta-C, diamond coatings, etc. Annealing leads to the effusion of hydrogen from a-C:H at 200–300 °C, graphitisation, and the release of internal stress [11,12,32]. Annealing of a Si-doped DLC coating in air causes the formation of a SiO_2 layer on top of the DLC, which results in good tribological properties at room and high temperatures [26,33].

High-energy oxygen plasma treatment such as reactive ion etching (RIE) can be used to etch the surface and modify the surface roughness [34,35]. Oxygen plasma etching of carbon-based coatings enhances the scratch resistance owing to sp^3 bond formation [36]. Improvements in the running-in properties and enhanced surface energy were found on low-energy oxygen plasma-treated ta-C specimens as compared with those treated with high-energy plasma [34]. This difference was explained by the interplay between the chemical reactions and physical collisions during irradiation. A reduced COF value was observed after the oxygen plasma treatment of a Si-doped DLC coating [37]. Improved tribological performance was also observed after the oxygen plasma treatment of a Si-free DLC coating [38]. Oxygen functional groups, including hydroxyl, were found on DLC coatings [38,39], and enhanced surface energy and hydrophilicity were reported after oxygen plasma treatment of DLC coatings [39].

The influence of nitrogen impurities on the structure and properties of DLC and ta-C coatings can be expected during annealing in ambient air and in sliding tests at high temperatures. The increase in the sp^2 bond content, release of the stress, and improvement in the adhesion to Si and CoCrMo alloys were revealed for nitrogen-doped DLC coatings [40,41].

The search strategy for systems exhibiting reduced friction and wear can involve investigating adaptive systems. These systems can self-organise (SO) under specific conditions [42,43]. Soft alloys such as babbitt alloys on relatively hard substrates can significantly increase the contact area, thus decreasing the contact pressure and wear rate at the initial stage of running-in. The initial period determines the tribological behaviour during the subsequent stages of sliding (hereditary effect). Thin oxide layers can have lower hardness (approximately 8.8 GPa for SiO_2 [44] and 10 GPa for amorphous Al_2O_3 [45]) than the DLC, ta-C, and diamond coatings; thus, they can be considered adaptive layers. For instance, it was found that the hardness of a Si-doped DLC coating after oxygen plasma treatment decreased owing to the formation of silicon oxide on top of the coating [37]. In conclusion, a thin silicon oxide film formed on top of a Si-doped DLC coating can be considered an adaptive layer with good lubricating properties that suppresses the atmospheric oxidation of the DLC coating. It should be stressed that different types of silicon oxide (Si_2O , SiO , Si_2O_3 , SiO_2) can be formed on Si-doped DLC coatings [46], and the role of each type of oxide should be specified in detail to explain these functionalities.

Alumina possesses many advantageous properties, including high thermal and chemical resistance and retained hardness at elevated temperatures [47]. A thin Al_2O_3 layer was deposited by atomic layer deposition (ALD) on nanocrystalline diamond (NCD) films, and improved oxidation resistance and thermal stability were demonstrated [48].

In the present preliminary study, a thin Al_2O_3 film (200 nm thick) deposited on top of an a-C:H:Si coating was considered an adaptive multifunctional layer. Improved tribological performance was expected because of modification of the contact conditions during running-in, delivery of extra oxygen into the contact area, reduction of hydrogen effusion, and suppression of the atmospheric oxidation of the a-C:H:Si coating.

2. Materials and Methods

The a-C:H:Si coatings were synthesised by plasma-activated chemical vapour deposition (PACVD) using an arc cathode physical vapour deposition (PVD) unit (Pi411) (PLATIT[®], Grenchen, Switzerland) with a PACVD option containing an MF bias supply (150–350 kHz range) and process gases (C_2H_2 and Si-containing precursor). The coating process started with Ar and metal ion etching, followed by Cr/CrN-based adhesion layer deposition via arc evaporation. The a-C:H:Si coating thickness and Si content in the coating were $1.0 \pm 0.1 \mu m$ and $<5 \text{ at.}\%$, respectively. Typical hardness values of a-C:H:Si were $26.5 \pm 1.5 \text{ GPa}$. The a-C:H:Si coating was deposited on polished WC-Co substrates ($\varnothing 13 \text{ mm}$, height 5 mm, $R_a = 0.05 \mu m$).

ALD was used to prepare Al_2O_3 films. The deposition was conducted in a flow-type reactor (Picosun R200, Espoo, Finland) at 300 °C using trimethylaluminum (TMA, $Al_2(CH_3)_6$) water as the precursor, and nitrogen as the purge gas. The pressure was

10 mbar (1 kPa). The precursor pulse lengths were 0.1/4/0.1/10 s for TMA/N₂/H₂O/N₂, respectively. After 2000 cycles, the thickness of the Al₂O₃ film was 200 nm. A spectroscopic ellipsometer (SemilabSopraGES-5E, Budapest, Hungary) was used to measure the film thickness, using 365 and 633 nm wavelengths at an angle of 75° on Si(100) reference substrates. Fitting was performed using the Cauchy approximation.

A ball-on-disc tribometer (Bruker[®] UMT-2, Billerica, MA, USA) equipped with a high-temperature chamber with a rotary drive was used to investigate the tribological behaviour of the specimens. Ø 10 mm Si₃N₄ balls (RedHill[®], Prague, Czech Republic) were used as counterbodies. The hardness, Young's modulus, and Poisson ratio of the balls were 1400–1700 HV, 310 GPa, and 0.27, respectively. Wear tests at RT and 400 °C were carried out on the a-C:H:Si and Al₂O₃/a-C:H:Si coatings. The normal load was 2 N, the speed of rotation was 200 rpm, and the wear track diameter was 3 mm. The samples were heated to 400 °C at a heating rate of 5 °C/min, and this temperature was stabilised for 45 min before the sliding test. In total, two sliding tests (for 180 and 5 min, respectively) for each type of specimen were carried out at RT. In the case of the tests at 400 °C, three tests were carried out (two for 180 min and one for 5 min) on the a-C:H:Si specimens and four tests (two for 180 min, one for 60 min, and one for 5 min) for the Al₂O₃/a-C:H:Si specimens. Humidity was 45% ± 5%.

The depth, width, and shape of the wear scars were investigated using stylus profilometry (Mahr Perthometer[®], Göttingen, Germany). Five line scans were taken across each wear scar, and an average line scan was obtained. The apparent volume (V) of the wear scar was estimated using the formula $V = S \times l$, where the cross-sectional area is S and the wear scar length is l .

Micro-Raman spectroscopy, X-ray photoelectron spectroscopy (XPS), and scanning electron microscopy (SEM) were used to evaluate the chemical structure and to monitor the morphology of the native and wear scar surfaces. Raman measurements were carried out using a Horiba LabRAM HR800 (Horiba[®], Kyoto, Japan) Micro-Raman system equipped with a cooled multichannel CCD detection system in the backscattering configuration with a spectral resolution better than 1 cm⁻¹. A Nd: YAG laser (wavelength $\lambda = 514$ nm) was used for excitation. The spot size was around 5 microns in diameter and spectra accumulation time was 60 s. The composition was studied using XPS in a Kratos Analytical AXIS ULTRA DLD (Kratos Analytical Ltd., Manchester, UK) spectrometer fitted with a monochromatic Al K _{α} X-ray source and an achromatic Mg K _{α} /Al K _{α} dual-anode X-ray source. A monochromatic Al K _{α} anode (1486.6 eV) operated at 150 W and 15 kV was used. A 180° hemispherical energy analyser with a mean radius of 165 mm was operated using a hybrid lens mode at a pass energy of 160 eV for survey spectra, 20 eV for regions, and 40 eV for regions acquired for the depth profile. XPS spectra were recorded at a 90° takeoff angle from the surface of the sample holder using an aperture field of view Ø 220 μ m. The samples were mounted on stainless steel 130 × 15 mm² sample bar. Binding energy values were calculated based on the C 1s peak at 284.6 eV. For surface cleaning and bulk composition information, a Minibeam I ion (Ar⁺) source (1 kV, 10 mA, 120 s per cycle) was used. The SEM images were taken using a (Zeiss EVO[®] MA—15 system, Oberkochen, Germany) with an LaB₆ cathode in secondary electron mode, applying an accelerating voltage of 10–15 kV and a 6.5–8.5 mm working distance.

3. Results

3.1. Morphology and Tribological Properties

Figure 1 shows the surface morphologies of the a-C:H:Si and Al₂O₃/a-C:H:Si coatings. The alumina layer grew conformally, that is, it resembled the morphology of the a-C:H:Si surface. Similar alumina growth was observed on the NCD film [48]. The morphological peculiarities can be observed on the Al₂O₃/a-C:H:Si coating surface.

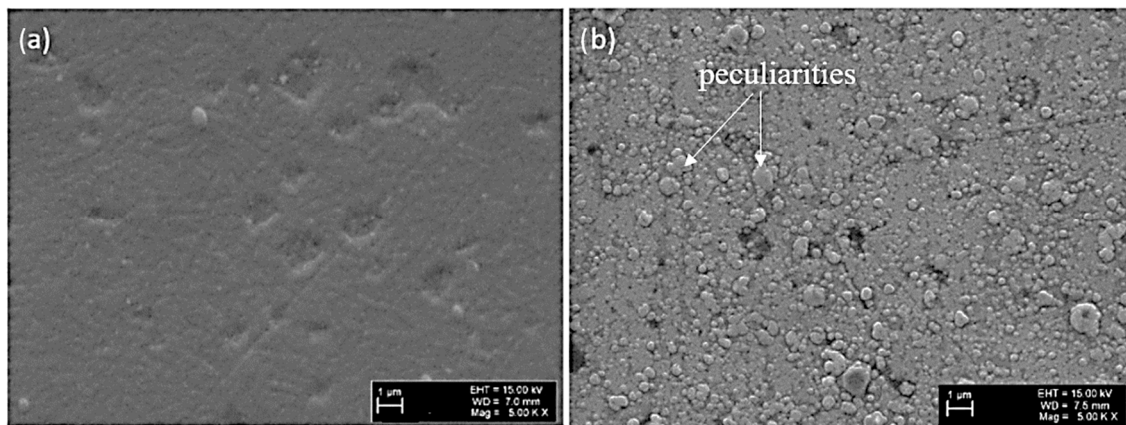


Figure 1. SEM images of the native surface of coatings (a) a-C:H:Si and (b) Al₂O₃/a-C:H:Si.

Figure 2 shows the COF versus cycle curves obtained at RT and 400 °C. The COF values for both types of specimens (a-C:H:Si and Al₂O₃/a-C:H:Si) are very similar for the tests at RT, approximately 0.06–0.1. In other words, the thin alumina layer did not strongly influence the friction behaviour of a-C:H:Si. After reaching the smallest value at the beginning of the test, the COF value slowly increased during subsequent periods of sliding. In contrast to the tests at RT, significant changes occurred in the tests at 400 °C. In the case of the a-C:H:Si coating, coating failure occurred at the beginning of the tests after a short running-in period. The tests were repeated three times (the 5 min test is not shown), and the same friction behaviour was observed. However, in the case of the Al₂O₃/a-C:H:Si coating, relatively stable periods of sliding were revealed, with a COF value of less than 0.03, and some periods had a super-low COF of less than 0.01 (Figure 2b). The extended time tests were repeated three times. A short running-in period was found in the case of the test at RT, which was practically absent from the tests at 400 °C. This shows that the contact between the a-C:H:Si surface and the Si₃N₄ ball was already established at the beginning of the tests.

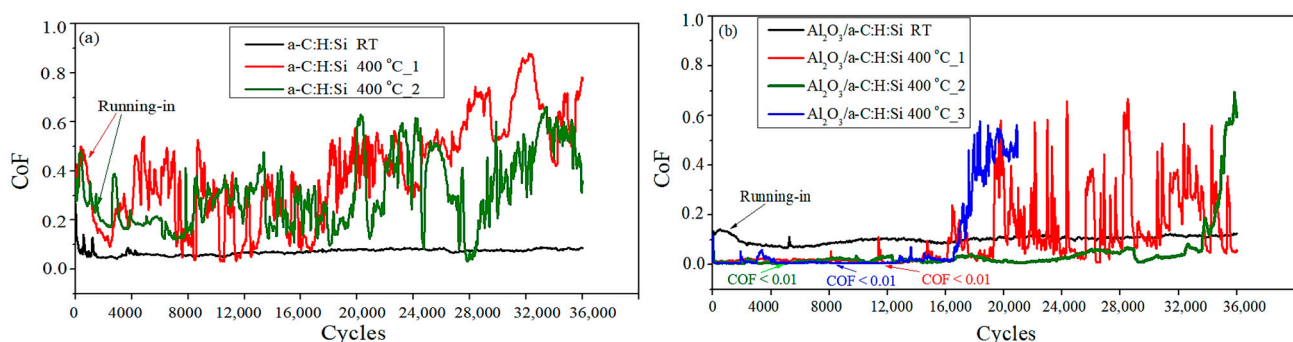


Figure 2. COF versus cycles curves taken on the (a) a-C:H:Si and (b) Al₂O₃/a-C:H:Si coatings.

Figure 3 shows SEM images of the wear scars observed on the a-C:H:Si and Al₂O₃/a-C:H:Si coatings after the sliding tests at RT and 400 °C. The smooth wear surfaces are formed on both coatings after sliding for 180 min at RT. The alumina islands can be seen on the Al₂O₃/a-C:H:Si coating as well (Figure 3b). In the case of the a-C:H:Si coating, islands of the a-C:H:Si coating and the surface of WC-Co substrate can be seen after the test at 400 °C, in spite of uniform a-C:H:Si coating surface for the Al₂O₃/a-C:H:Si specimen.

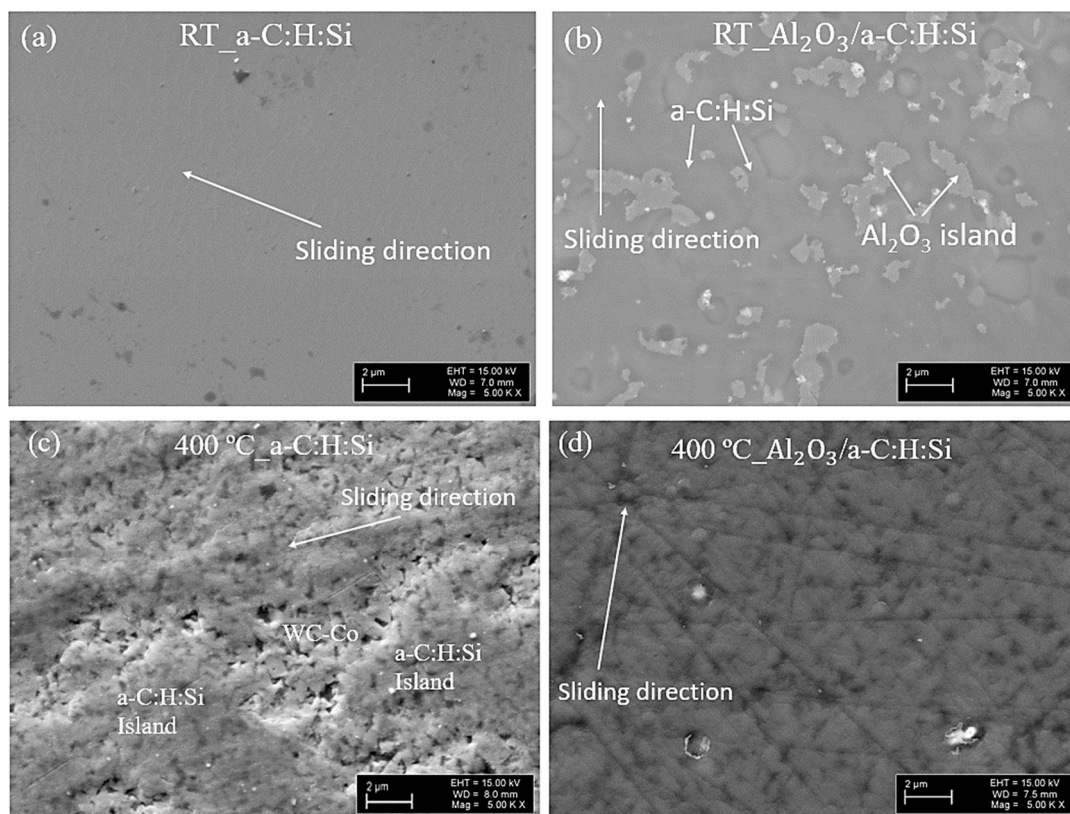


Figure 3. SEM images of wear scars after sliding tests at (a,b) RT for 180 min and (c,d) 400 °C for 5 min.

Figure 4 shows line scans taken across the wear scars. The shape and width of the wear scars obtained after the tests at RT differ between the a-C:H:Si and Al₂O₃/a-C:H:Si coatings. The wear scar widths on the a-C:H:Si and Al₂O₃/a-C:H:Si coatings after the 5-min tests were approximately 200 and 310 μm, respectively. The wear scar was narrower and deeper for the a-C:H:Si specimen and wider and shallower for Al₂O₃/a-C:H:Si after the 180-min tests. The increase in contact area on Al₂O₃/NCD in contrast to an NCD film was also observed in sliding tests at RT [48]. These results demonstrate the adaptation effect mentioned earlier, that is, that an increase in the contact area leads to decreasing contact pressure. The hardness of the Si₃N₄ balls was higher than that of the thin alumina layer, thus it is unlikely that the increased wear scar width was caused by abrasive wear of the balls. The depth of the wear scar was approximately 0.8 μm for the a-C:H:Si coating, which is close to the coating thickness. However, in the case of the Al₂O₃/a-C:H:Si coating, an approximately 0.4 μm-thick a-C:H:Si layer was removed (Figure 4d).

Therefore, a longer lifetime can be expected for the Al₂O₃/a-C:H:Si coating in contrast to the a-C:H:Si coating at RT. The wear scar was also significantly wider after the 5 min test at 400 °C than after the 180 min test at RT for the Al₂O₃/a-C:H:Si coating (Figures 4d and 5b). These results could indicate structural changes within the a-C:H:Si coating, most likely owing to a-C:H:Si graphitisation and decreased hardness [11,26].

The apparent wear volumes were measured on the a-C:H:Si and Al₂O₃/a-C:H:Si specimens (Figure 6). The calculation of the wear volume loss assumed an alumina layer thickness of 200 nm (Figures 4 and 5). The wear volume measured on the a-C:H:Si layer (black colour in Figure 6) was larger for the a-C:H:Si coating than for the Al₂O₃/a-C:H:Si coating after the 180 min tests at RT. The wear volume was largest after the 5 min sliding test at 400 °C on the a-C:H:Si coating owing to the coating failure (Figure 5a). It should be stressed that the reduced hardness of a-C:H:Si at high temperature increased the wear scar width for the Al₂O₃/a-C:H:Si coating (Figure 5b). Therefore, the apparent wear volume loss may increase owing to the plastic deformation of the a-C:H:Si layer [49].

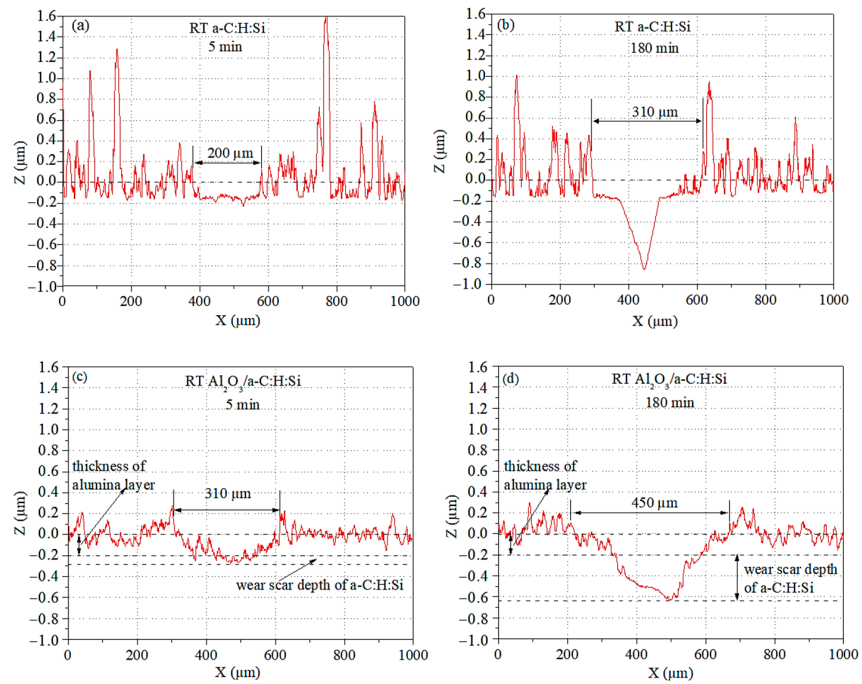


Figure 4. Wear scars line profiles taken on the (a,b) a-C:H:Si and (c,d) Al₂O₃/a-C:H:Si coatings after the (a,c) 5 and (b,d) 180 min tests at RT.

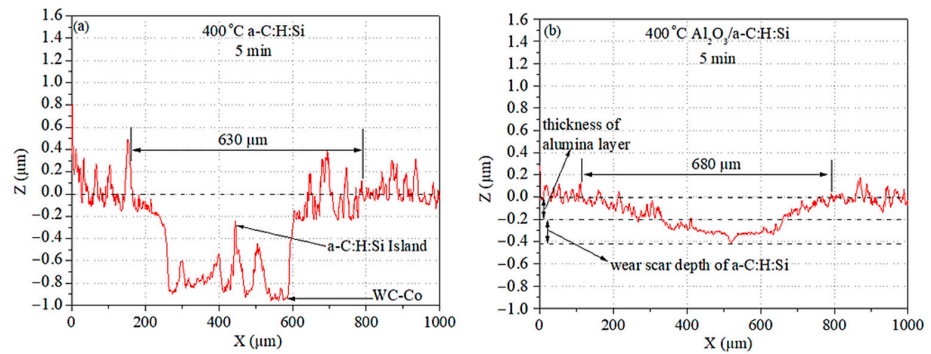


Figure 5. Wear scars line profiles taken on the (a) a-C:H:Si and (b) Al₂O₃/a-C:H:Si coatings after the 5 min sliding tests at 400 °C.

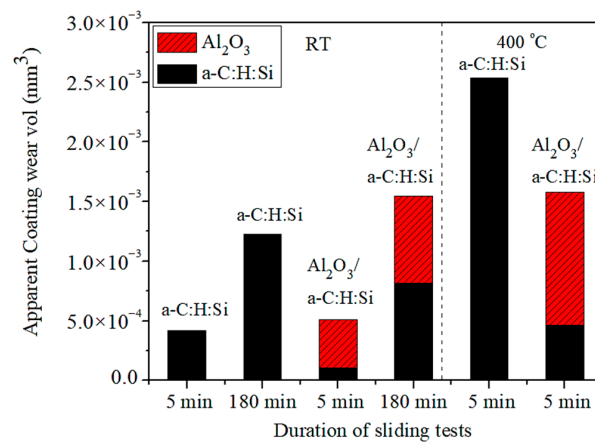


Figure 6. Apparent wear volumes measured on the a-C:H:Si and Al₂O₃/a-C:H:Si coatings.

3.2. Raman and XPS Analyses

Raman spectra were obtained for the native and wear scar surfaces of the a-C:H:Si coating after the sliding tests at RT (Figure 7a). Two characteristic D and G peaks indicated sp^2 structure ordering, that is, the D mode (1365 cm^{-1}) was active in the presence of disorder, and the G mode (1545 cm^{-1}) indicated the presence of well-ordered graphite [6]. Raman peaks corresponding to vibrational modes in t-Pa (1054 cm^{-1}) and sp -bonded chains ($1900\text{--}2200\text{ cm}^{-1}$) were also observed. The shape and position of the Raman peaks in the spectra of the native and wear scar surfaces after the 5 and 180 min tests at RT were quite similar. In the case of the $\text{Al}_2\text{O}_3/\text{a-C:H:Si}$ coating (Figure 7c), the peak positions were similar to those observed for the a-C:H:Si coating, except that the G peak shifted to 1532 cm^{-1} after the 180 min sliding test. The Raman spectrum of the native a-C:H:Si surface differed from that after heating at high temperatures. The G peak shifted to 1558 cm^{-1} , and formation of a shoulder (arrow in Figure 7b) was observed after heating at $400\text{ }^\circ\text{C}$. The G peak shifted to a higher value (1612 cm^{-1}) after the 5 min test at $400\text{ }^\circ\text{C}$ (Figure 7b), which indicates the impact of mechanochemical processes on the a-C:H:Si structure. For the sake of clarity, Raman measurements were repeated for at least three different locations within the wear scar, and similar spectra were recorded (Figure 7b). However, in the case of the $\text{Al}_2\text{O}_3/\text{a-C:H:Si}$ coating, no further G peak shift was observed after the 5 min test at $400\text{ }^\circ\text{C}$ (Figure 7d). The peak positions and shapes were similar to those observed in the Raman spectrum of the native surface of the a-C:H:Si coating after heating at $400\text{ }^\circ\text{C}$ (Figure 7b).

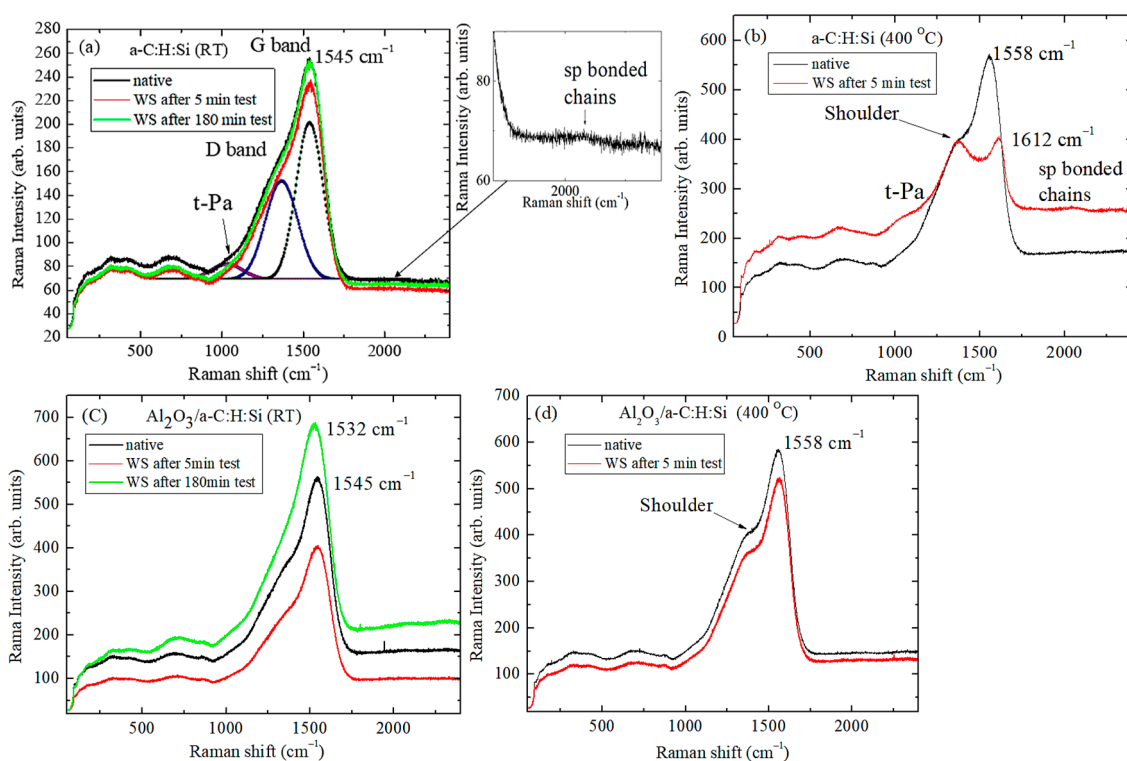


Figure 7. Raman spectra taken on the native surface and within the wear scars after the 5 and 180 min tests at RT and $400\text{ }^\circ\text{C}$ on the (a,b) a-C:H:Si and (c,d) $\text{Al}_2\text{O}_3/\text{a-C:H:Si}$ coatings. The insert shows the peak $1900\text{--}2200\text{ cm}^{-1}$ corresponding to sp -bonded chains. Deconvolution of Raman spectra of the native a-C:H:Si is shown.

The C 1s XPS spectra were recorded on the a-C:H:Si native surface (Figure 8). The peaks corresponded to C–C sp^2 , C–C sp^3 , C–O, C=O, C–N, O–C=O and COO–R bonds [46,50,51]. Sp^3 surface enrichment and increased intensity of the XPS spectrum shoulder corresponding to the bonds formed between carbon, nitrogen, and oxygen atoms were observed after heating at $400\text{ }^\circ\text{C}$ (Figure 8b). Figure 9 shows the XPS spectra taken on the surface of the wear scars after the sliding tests at RT and $400\text{ }^\circ\text{C}$. The intensity

ratio between the XPS signal intensity related to the a-C:H:Si coating (convolution of the C–C sp^2 and sp^3 peaks) and the intensity of the peak corresponding to C–O, C=O, etc., bonds is higher for a-C:H:Si than for the $Al_2O_3/a-C:H:Si$ coating. The C–C sp^2 and sp^3 XPS signals can be more strongly shielded on the $Al_2O_3/a-C:H:Si$ coating by a thicker and more uniformly distributed layer formed by agents such as C–O, C=O, etc.

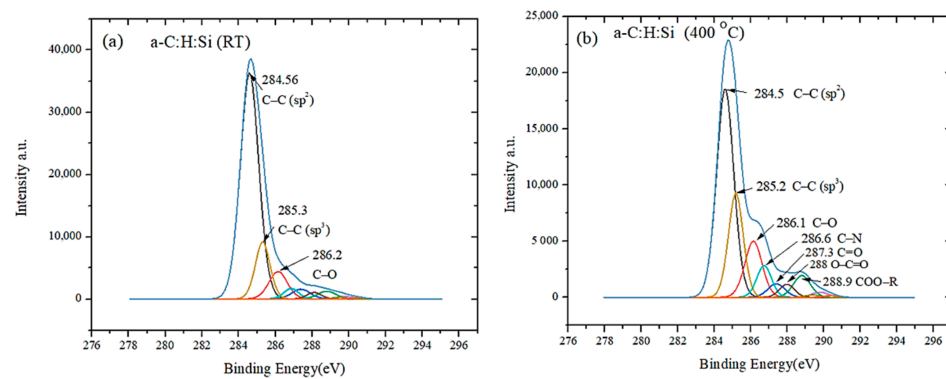


Figure 8. C1s XPS spectra taken on the a-C:H:Si coating native surface at (a) RT and (b) 400 °C.

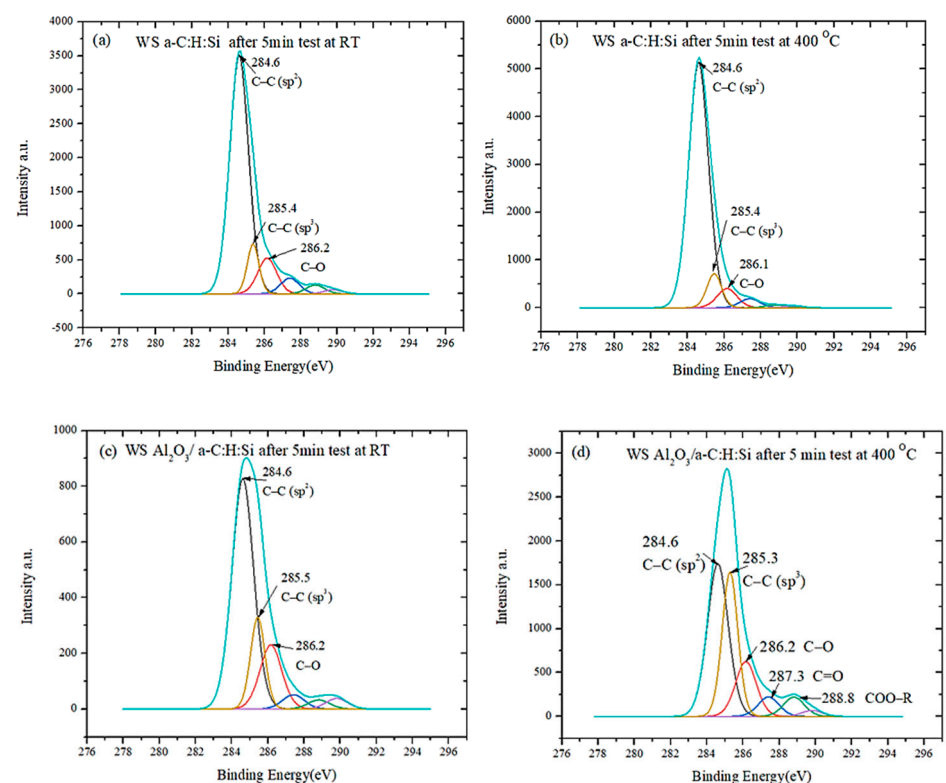


Figure 9. C 1s XPS spectra taken within the wear scars after the 5 min tests at RT and 400 °C on the (a,b) a-C:H:Si and (c,d) $Al_2O_3/a-C:H:Si$ coatings.

Figures 10 and 11 show the O 1s and Si 2p XPS spectra, respectively. The O 1s XPS spectra were quite similar for both types of specimens. It is expected that the XPS signal indicates electrons released from oxygen bonded mainly with C, H, Si, Al, and N atoms. The stronger peak at 531.6 eV after the heating of a-C:H:Si at 400 °C can be observed in contrast to the $Al_2O_3/a-C:H:Si$ coating. Closely spaced spin-orbit components ($\Delta = 0.63$ eV) formed an asymmetrical Si 2p peak at 100.5–100.6 eV, which corresponds to Si–C bonds in a-C:H:Si [52]. The broad Si 2p XPS spectra indicate the presence of several types of silicon oxide with different chemical states of Si ($Si^{1+}(Si_2O)$, $Si^{2+}(SiO)$, $Si^{3+}(Si_2O_3)$, and

$\text{Si}^{4+}(\text{SiO}_2)$ [46]. Due to the likely a-C:H:Si oxidation and formation of the silicon oxides, the Si–C peak intensity decreased after heating at 400 °C (Figure 11a). The Si 2p XPS spectra taken within the wear scars after the sliding test at 400 °C showed the strongest peaks located at 102.5–103.2 eV, which could indicate the formation of stoichiometric SiO_2 oxide. However, there is a difference between the Si 2p XPS spectra of the a-C:H:Si and $\text{Al}_2\text{O}_3/\text{a-C:H:Si}$ coatings (Figure 11a,b, respectively). For example, the strongest peak in the spectrum taken on the $\text{Al}_2\text{O}_3/\text{a-C:H:Si}$ surface is located at 102.5 eV, in contrast to 103.2 eV for a-C:H:Si. The Si 2p XPS spectra may also have been influenced by the Si_3N_4 ball wear debris during the sliding tests.

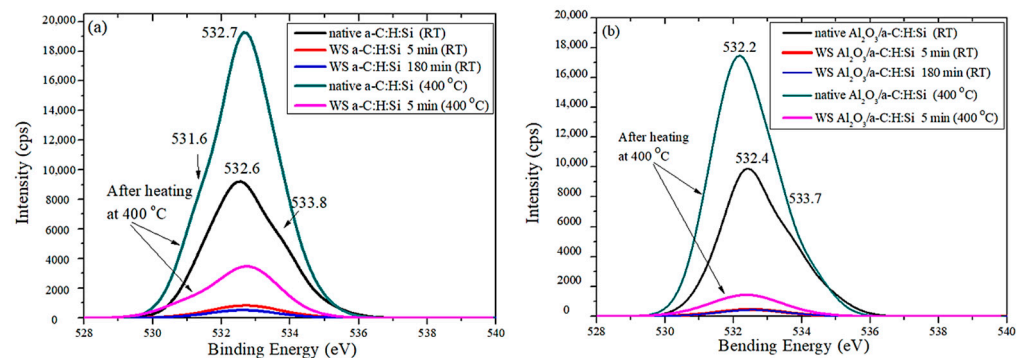


Figure 10. O 1s XPS spectra taken within the native and wear scars surfaces after sliding tests at RT and 400 °C on the (a) a-C:H:Si and (b) $\text{Al}_2\text{O}_3/\text{a-C:H:Si}$ coatings.

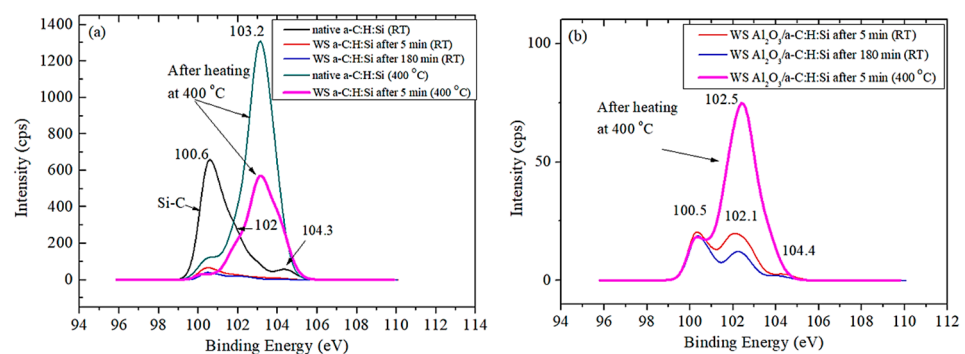


Figure 11. Si 2p XPS spectra taken within the native and wear scars surfaces after the sliding tests at RT and 400 °C on the (a) a-C:H:Si and (b) $\text{Al}_2\text{O}_3/\text{a-C:H:Si}$ coatings.

Figure 12 shows the N 1s XPS spectra. In the case of the a-C:H:Si coating, the peak at 402.1 eV (N–O) [51] was observed after the 5 min sliding test at 400 °C.

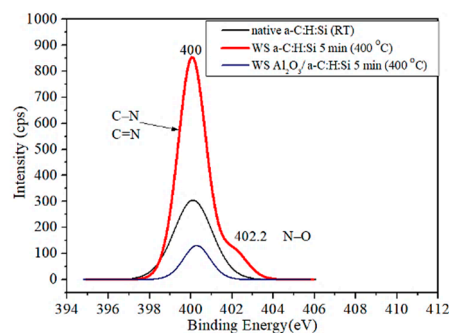


Figure 12. N 1s XPS spectra taken within the native and wear scars surfaces after the 5 min tests at RT and 400 °C on the a-C:H:Si and $\text{Al}_2\text{O}_3/\text{a-C:H:Si}$ coatings.

4. Discussion

Figure 13 shows the results of the Raman and XPS investigations of the sp^2 and sp^3 bond contents in the coatings. In the case of the a-C:H:Si coating, the intensity ratios of the D and G peaks (I_D/I_G ratio) are similar for the Raman spectra taken on the native surface and within the wear scars after the 5 and 180 min sliding tests at RT (Figure 13a). For the same specimens, the sp^2/sp^3 ratios of the corresponding XPS peak intensities were similar (Figure 13b). Therefore, these results suggest that mechanochemical processes occurring during sliding tests at RT did not affect the sp^2 and sp^3 hybridised bonding networks in the bulk and on the surface of the a-C:H:Si coating. This demonstrates the high stability of the a-C:H:Si structure in sliding tests at RT. However, the investigation of the a-C:H:Si native surface after heating at 400 °C shows that the sp^2 and sp^3 contents in the bulk and on the surface changed in different ways. In contrast to the investigations at RT, the analysis of the I_D/I_G ratio suggests an increase in the sp^2 content in the bulk; however, the XPS data showed a decrease in the sp^2 content on the surface and sp^3 surface enrichment. The sp^3 surface enrichment after annealing in air owing to preferable etching of the sp^2 bonds located within the grain boundaries has been found on diamond films [48,53]. The release of carbon from the a-C:H:Si surface during annealing at 400 °C was observed by Rouhani et al. [46].

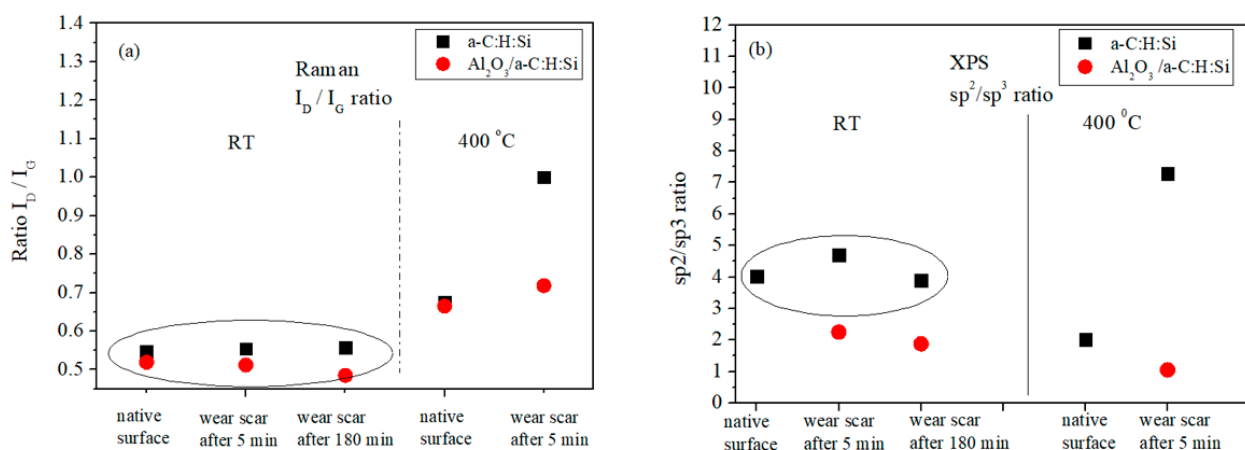


Figure 13. Summary of the results of (a) Raman and (b) XPS investigations.

In the case of the Al₂O₃/a-C:H:Si coating, comparison of the I_D/I_G ratios obtained for the native and wear scar surfaces after the 5 and 180 min tests showed that this ratio also remained stable at RT (Figure 13a). However, the I_D/I_G ratio tended to decrease for the 180 min test as compared with the measurements on the native surface and wear scar after the 5 min test, which indicates likely surface sp^3 enrichment within the wear scar. The XPS investigation supports this conclusion (Figure 13b), as well as the G peak shift to 1532 cm⁻¹ observed after 180 min (Figure 7c). The extra oxygen delivered by the alumina layer seems to have caused surface sp^3 enrichment in the wear scars after the sliding tests at RT on the Al₂O₃/a-C:H:Si coating owing to mechanochemical processes. This conclusion is in good agreement with the increased sp^3 bond content in the oxygen-doped carbon-based coating [31,36].

In the case of the a-C:H:Si and Al₂O₃/a-C:H:Si coatings, the increased I_D/I_G ratio suggests an increase in the sp^2 content for both types of specimens after the 5 min tests at 400 °C (Figure 13a). The thermally and mechanochemically induced processes intensified the a-C:H:Si graphitisation. However, the increase in the sp^2 bond content was significantly higher for the a-C:H:Si coating than for Al₂O₃/a-C:H:Si coating, and a shift of the G peak to 1612 cm⁻¹ was observed for the a-C:H:Si coating (Figure 7b). This shift could indicate an increase in the number of defects, formation of a graphene sheet owing to graphite slicing, and formation of double bonds between carbon atoms [54]. There was a significant

difference between the a-C:H:Si and Al₂O₃/a-C:H:Si coatings, namely, sp³ enrichment of the wear scar surface on the Al₂O₃/a-C:H:Si coating after the 5 min test at 400 °C (Figure 13b).

The results of the Raman and XPS investigations suggest that the interaction between the a-C:H:Si surface and atmospheric oxygen differed from the interaction with the oxygen in alumina. It is expected that the alumina layer suppressed atmospheric oxygen diffusion to the a-C:H:Si surface [48].

To summarise, improvements in the tribological properties and thermal stability were observed in sliding tests at RT and 400 °C for the Al₂O₃/a-C:H:Si coating in comparison with the a-C:H:Si coating. First, an increase in the contact area and sp³ surface enrichment within the wear scar was observed in the tests at RT and 400 °C. The alumina layer was considered the adaptive layer. The adaptation effect was manifested owing to the use of a relatively soft and thin alumina layer, resulting in the increased contact area. The delivery of extra oxygen to the contact area led to increased sp³ content within the thin tribolayer, which improved the thermal stability and increased the hardness and internal stress of the tribolayer [28–31,36]. In addition, it was shown in a study on an Al₂O₃/NCD film [48] that the alumina layer is the atmospheric oxygen diffusion barrier layer. These factors determine the running-in conditions and tribological performance during extended time tests (hereditary effects). The decreased contact pressure owing to the increased contact area and improved mechanical properties of the thin tribolayer led to the better tribological behaviour of Al₂O₃/a-C:H:Si coating in contrast to the a-C:H:Si coating.

Second, carbon surface hydroxylation (C–OH termination) results in better tribological properties [38]. This type of surface passivation improves surface hydrophilicity and the absorption of atmospheric water vapour [39]. The super-low COF value for the a-C:H:Si coating with a low Si concentration (3.6 at.%–11.4 at.%) is explained by the formation of additional Si–OH hydrophilic bonds. Under ambient humid conditions (30%–60% humidity), water and oxygen absorbed by the surface form a well-ordered easily shared layer-like film, resulting in low friction [17]. In addition, higher surface energies for a-C:H:Si and ta-C coating surfaces after oxygen plasma treatment have been reported [34,39], which means higher surface wettability, which leads to more uniform water distribution along the surface. This, in turn, is likely to be beneficial for the formation of a layer-like water structure on the a-C:H:Si surface. In conclusion, it is expected that the hydrophilicity and wettability of Al₂O₃/a-C:H:Si within the wear scar area can be improved owing to the extra oxygen delivered by the alumina layer. This interpretation is supported by the XPS investigation, as discussed in Section 3.2.

Third, silicon oxide affects the tribological behaviour of DLC coatings. The XPS study revealed several types of silicon oxide formed within the wear scar. The influence of a particular type of oxide should be investigated in more detail.

Fourth, the mechanism of hydrogen effusion may differ between the a-C:H:Si and Al₂O₃/a-C:H:Si coatings because of the alumina layer and a specific tribolayer layer formed on Al₂O₃/a-C:H:Si during the sliding tests. Upon thermal treatment, the hydrogen content decreases owing to the release of hydrogen and hydrocarbons (C_nH_x) [32]. The mechanisms of hydrogen diffusion in alumina usually consider the diffusion of H atoms or H⁺ ions [55]. The hydrogen diffusion coefficient in alumina has a certain value; therefore, the hydrogen effusion in the Al₂O₃/a-C:H:Si coating can be suppressed by the alumina layer. In the case of hydrocarbons, it was found that the pore size in a-C:H strongly influences diffusion [32]. Thus, hydrocarbon diffusion through alumina can be limited as well. In conclusion, the alumina layer can be considered a hydrogen diffusion barrier layer.

5. Conclusions

A comparative study of the tribological properties of the a-C:H:Si and Al₂O₃/a-C:H:Si coatings at RT and 400 °C was performed. After 180 min sliding tests at RT, a wider and shallower wear scar was found on the Al₂O₃/a-C:H:Si coating in contrast to the a-C:H:Si coating. The smaller depth indicates that the a-C:H:Si coating lifetime can be increased by

preparing an Al₂O₃/a-C:H:Si structure. The alumina layer changes the contact conditions and influences the running-in behaviour owing to the increased contact area and decreased contact pressure (adaptation effect). The chemical composition in the contact area can also be changed owing to the extra oxygen delivered by the alumina layer. The results demonstrate the hereditary effect and the initial contact conditions strongly influence the tribological performance of the extended time tests.

The thermal stability of the a-C:H:Si coating can be improved by deposition of an alumina layer. The a-C:H:Si coating was unstable in sliding tests at 400 °C; however, a stable low-friction regime of sliding over 80–160 min was observed for the Al₂O₃/a-C:H:Si coating. The chemical composition of the tribolayer on Al₂O₃/a-C:H:Si differed from that of the a-C:H:Si coating after the sliding tests at 400 °C. An increase in the sp³ bond content was observed for the Al₂O₃/a-C:H:Si coating; therefore, better mechanical and thermal properties of the tribolayer formed on an Al₂O₃/a-C:H:Si coating are expected. The extra oxygen in the contact area improved the structure and properties of the passivation layer formed on the a-C:H:Si surface, resulting in low friction.

Further investigations are needed to continue efforts towards understanding the mutual influence between the test conditions and the DLC and alumina layer properties.

Author Contributions: Conceptualization, V.P. and A.A.; methodology, V.P.; software, A.A. and M.Y.; validation, A.B. and A.A.; formal analysis, V.P.; and A.A.; investigation, A.A.; T.J.; T.R.; M.V. and M.D.; resources, V.P.; data curation, A.A.; writing—original draft preparation, V.P.; and A.A.; writing—review and editing, F.S.; J.S.; A.L.; and J.K.; visualization, A.A.; supervision, V.P.; project administration, V.P.; funding acquisition, V.P. All authors have read and agreed to the published version of the manuscript.

Funding: This research was funded by the Estonian Ministry of Education and Research under financing projects PUT 1369 and TK134 “Emerging orders in quantum and nanomaterials”.

Institutional Review Board Statement: Not applicable.

Informed Consent Statement: Not applicable.

Data Availability Statement: Not applicable.

Conflicts of Interest: The authors declare no conflict of interest.

References

- Holmberg, K.; Erdemir, A. Influence of tribology on global energy consumption, costs and emissions. *Friction* **2017**, *5*, 263–284. [[CrossRef](#)]
- Kowalski, S. The influence of selected PVD coatings on fretting wear in a clamped joint based on the example of a rail vehicle wheel set. *Eksploatacja Niezawodn. Maint. Reliab.* **2017**, *20*, 1–8. [[CrossRef](#)]
- Rybachuk, M.; Bell, J. Electronic states of trans-polyacetylene, poly(p-phenylene vinylene) and sp-hybridised carbon species in amorphous hydrogenated carbon probed by resonant Raman scattering. *Carbon* **2009**, *47*, 2481–2490. [[CrossRef](#)]
- Mulazzi, E.; Brivio, G.P.; Faulques, E.; Lefrant, S. Experimental and theoretical Raman results in transpolyacetylene. *Solid State Commun.* **1983**, *46*, 851–855. [[CrossRef](#)]
- Ravagnan, L.; Manini, N.; Cinquanta, E.; Onida, G.; Sangalli, D.; Motta, C.; Devetta, M.; Bordoni, A.; Piseri, P.; Milani, P. Effect of axial torsion on sp carbon atomic wires. *Phys. Rev. Lett.* **2009**, *102*, 245502. [[CrossRef](#)]
- Ferrari, A.C.; Robertson, J. Raman spectroscopy of amorphous, nanostructured, diamond-like carbon, and nanodiamond. *Philos. Trans. R. Soc. A Math. Phys. Eng. Sci.* **2004**, *362*, 2477–2512. [[CrossRef](#)]
- Hilbert, J.; Mangolini, F.; McClimon, J.; Lukes, J.; Carpick, R. Si doping enhances the thermal stability of diamond-like carbon through reductions in carbon-carbon bond length disorder. *Carbon* **2018**, *131*, 72–78. [[CrossRef](#)]
- Dongping, L.; Baoxiang, C.; Yanhong, L. Structures of diamond-like carbon films. *Plasma Sci. Technol.* **2006**, *8*, 285–291. [[CrossRef](#)]
- Kalish, R.; Lifshitz, Y.; Nugent, K.; Praver, S. Thermal stability and relaxation in diamond-like-carbon. A Raman study of films with different sp³ fractions (ta-C to a-C). *Appl. Phys. Lett.* **1999**, *74*, 2936–2938. [[CrossRef](#)]
- Rybachuk, M.; Bell, J.M. The effect of sp² fraction and bonding disorder on micro-mechanical and electronic properties of a-C:H films. *Thin Solid Film.* **2007**, *515*, 7855–7860. [[CrossRef](#)]
- Li, H.; Xu, T.; Wang, C.; Chen, J.; Zhou, H.; Liu, H. Annealing effect on the structure, mechanical and tribological properties of hydrogenated diamond-like carbon films. *Thin Solid Film.* **2006**, *515*, 2153–2160. [[CrossRef](#)]
- Tallant, D.; Parmeter, J.; Siegal, M.; Simpson, R. The thermal stability of diamond-like carbon. *Diam. Relat. Mater.* **1995**, *4*, 191–199. [[CrossRef](#)]

13. Pastewka, L.; Moser, S.; Gumbsch, P.; Moseler, M. Anisotropic mechanical amorphization drives wear in diamond. *Nat. Mater.* **2010**, *10*, 34–38. [[CrossRef](#)] [[PubMed](#)]
14. Yu, Q.; Chen, X.; Zhang, C.; Luo, J. Influence factors on mechanisms of superlubricity in DLC films: A review. *Front. Mech. Eng.* **2020**, *6*, 65. [[CrossRef](#)]
15. Țucureanu, V.; Matei, A.; Avram, A.M. FTIR spectroscopy for carbon family study. *Crit. Rev. Anal. Chem.* **2016**, *46*, 502–520. [[CrossRef](#)] [[PubMed](#)]
16. Fontaine, J.; Loubet, J.L.; Mogne, T.L.; Grill, A. Superlow friction of diamond-like carbon films: A relation to viscoplastic properties. *Tribol. Lett.* **2004**, *17*, 709–714. [[CrossRef](#)]
17. Chen, X.; Kato, T.; Kawaguchi, M.; Nosaka, M.; Choi, J. Structural and environmental dependence of superlow friction in ion vapour-deposited a-C:H:Si films for solid lubrication application. *J. Phys. D Appl. Phys.* **2013**, *46*, 255304. [[CrossRef](#)]
18. Kano, M.; Yasuda, Y.; Okamoto, Y.; Mabuchi, Y.; Hamada, T.; Ueno, T.; Ye, J.; Konishi, S.; Takeshima, S.; Martin, J.M.; et al. Ultralow friction of DLC in presence of glycerol mono-oleate (GNO). *Tribol. Lett.* **2005**, *18*, 245–251. [[CrossRef](#)]
19. Holmberg, K.; Ronkainen, H.; Laukkanen, A.; Wallin, K. Friction and wear of coated surfaces—Scales, modelling and simulation of tribomechanisms. *Surf. Coat. Technol.* **2007**, *202*, 1034–1049. [[CrossRef](#)]
20. Erdemir, A. The role of hydrogen in tribological properties of diamond-like carbon films. *Surf. Coat. Technol.* **2001**, *146*–147, 292–297. [[CrossRef](#)]
21. Zeng, Q.; Eryilmaz, O.; Erdemir, A. Superlubricity of the DLC films-related friction system at elevated temperature. *RSC Adv.* **2015**, *5*, 93147–93154. [[CrossRef](#)]
22. Kano, M.; Martin, J.M.; Yoshida, K.; Bouchet, M.I.D.B. Super-low friction of ta-C coating in presence of oleic acid. *Friction* **2014**, *2*, 156–163. [[CrossRef](#)]
23. Kuwahara, T.; Romero, P.A.; Makowski, S.; Weihnacht, V.; Moras, G.; Moseler, M. Mechano-chemical decomposition of organic friction modifiers with multiple reactive centres induces superlubricity of ta-C. *Nat. Commun.* **2019**, *10*, 151. [[CrossRef](#)]
24. Ikeyama, M.; Nakao, S.; Miyagawa, Y. Effects of Si content in DLC films on their friction and wear properties. *Surf. Coat. Technol.* **2005**, *191*, 38–42. [[CrossRef](#)]
25. Baba, K.; Hatada, R.; Flege, S.; Ensinger, W. Deposition of silicon-containing diamond-like carbon films by plasma-enhanced chemical vapour deposition. *Surf. Coat. Technol.* **2009**, *203*, 2747–2750. [[CrossRef](#)]
26. Zhang, T.F.; Wan, Z.X.; Ding, J.C.; Zhang, S.; Wang, Q.M.; Kim, K.H. Microstructure and high-temperature tribological properties of Si-doped hydrogenated diamond-like carbon films. *Appl. Surf. Sci.* **2018**, *435*, 963–973. [[CrossRef](#)]
27. Wang, J.; Pu, J.; Zhang, G.; Wang, L. Interface architecture for superthick carbon-based films toward low internal stress and ultrahigh load-bearing capacity. *ACS Appl. Mater. Interfaces* **2013**, *5*, 5015–5024. [[CrossRef](#)] [[PubMed](#)]
28. Moolsradoo, N.; Abe, S.; Watanabe, S. Thermal stability and tribological performance of DLC-Si-O films. *Adv. Mater. Sci. Eng.* **2011**, *2011*, 1–7. [[CrossRef](#)]
29. Mangolini, F.; Krick, B.A.; Jacobs, T.D.; Khanal, S.R.; Streller, F.; McClimon, J.B.; Hilbert, J.; Prasad, S.V.; Scharf, T.W.; Ohlhausen, J.A.; et al. Effect of silicon and oxygen dopants on the stability of hydrogenated amorphous carbon under harsh environmental conditions. *Carbon* **2018**, *130*, 127–136. [[CrossRef](#)]
30. Zhang, D.; Li, S.; Zuo, X.; Guo, P.; Ke, P.; Wang, A. Structural and mechanism study on enhanced thermal stability of hydrogenated diamond-like carbon films doped with Si/O. *Diam. Relat. Mater.* **2020**, *108*, 107923. [[CrossRef](#)]
31. Safaie, P.; Eshaghi, A.; Bakhshi, S.R. Structure and mechanical properties of oxygen doped diamond-like carbon thin films. *Diam. Relat. Mater.* **2016**, *70*, 91–97. [[CrossRef](#)]
32. Wild, C.; Koidl, P. Thermal gas effusion from hydrogenated amorphous carbon films. *Appl. Phys. Lett.* **1987**, *51*, 1506–1508. [[CrossRef](#)]
33. Yang, B.; Zheng, Y.; Zhang, B.; Wei, L.; Zhang, J. The high-temperature tribological properties of Si-DLC films. *Surf. Interface Anal.* **2012**, *44*, 1601–1605. [[CrossRef](#)]
34. Kim, J.-I.; Jang, Y.-J.; Kim, J.; Jeong, J.H. Improvement of running-in process of tetrahedral amorphous carbon film sliding against Si₃N₄ under humid air by O₂ plasma post-irradiation. *Appl. Surf. Sci.* **2021**, *538*, 147957. [[CrossRef](#)]
35. Fredriksson, H.; Chakarov, D.; Kasemo, B. Patterning of highly oriented pyrolytic graphite and glassy carbon surfaces by nanolithography and oxygen plasma etching. *Carbon* **2009**, *47*, 1335–1342. [[CrossRef](#)]
36. Guo, M.; Diao, D.; Fan, X.; Yang, L.; Yu, L. Scratch behavior of re-structured carbon coating by oxygen plasma etching technology for magnetic disk application. *Surf. Coat. Technol.* **2014**, *251*, 128–134. [[CrossRef](#)]
37. Choi, J.; Nakao, S.; Ikeyama, M.; Kato, T. Effect of oxygen plasma treatment on the tribological properties of Si-DLC coatings. *Phys. Status Solid* **2008**, *5*, 956–959. [[CrossRef](#)]
38. Jongwannasiri, C.; Watanabe, S. Tribological behavior of O₂ and CF₄ plasma post-treated diamond-like carbon films under dry air and in a high relative humidity environment. *Surf. Coat. Technol.* **2016**, *306*, 200–204. [[CrossRef](#)]
39. López-Santos, C.; Yubero, F.; Cotrino, J.; González-Elipe, A. Lateral and in-depth distribution of functional groups on diamond-like carbon after oxygen plasma treatments. *Diam. Relat. Mater.* **2011**, *20*, 49–56. [[CrossRef](#)]
40. Corona-Gomez, J.; Shiri, S.; Mohammadtaheri, M.; Yang, Q. Adhesion enhancement of DLC on CoCrMo alloy by diamond and nitrogen incorporation for wear resistant applications. *Surf. Coat. Technol.* **2017**, *332*, 120–127. [[CrossRef](#)]
41. Rao, X.; Yang, J.; Chen, Z.; Yuan, Y.; Chen, Q.; Feng, X.; Qin, L.; Zhang, Y. Tuning C–C sp²/sp³ ratio of DLC films in FCVA system for biomedical application. *Bioact. Mater.* **2020**, *5*, 192–200. [[CrossRef](#)]

42. Fox-Rabinovich, G.S. Principles of friction control for surface-engineered materials. In *Self-Organization during Friction. Advanced Surface-Engineered Materials and Systems Design*; Fox-Rabinovich, G.S., Totten, G.E., Eds.; CRC Press: Boca Raton, FL, USA, 2006; pp. 3–12.
43. Podgursky, V.; Bogatov, A.; Yashin, M.; Sobolev, S.; Gershman, I.S. Relation between self-organization and wear mechanisms of diamond films. *Entropy* **2018**, *20*, 279. [[CrossRef](#)] [[PubMed](#)]
44. Li, H.; Vlassak, J.J. Determining the elastic modulus and hardness of an ultra-thin film on a substrate using nanoindentation. *J. Mater. Res.* **2009**, *24*, 1114–1126. [[CrossRef](#)]
45. Jõgiaas, T.; Zabels, R.; Tamm, A.; Merisalu, M.; Hussainova, I.; Heikkilä, M.; Mändar, H.; Kukli, K.; Ritala, M.; Leskelä, M. Mechanical properties of aluminum, zirconium, hafnium and tantalum oxides and their nanolaminates grown by atomic layer deposition. *Surf. Coat. Technol.* **2015**, *282*, 36–42. [[CrossRef](#)]
46. Rouhani, M.; Hogley, J.; Hong, F.C.-N.; Jeng, Y.-R. Spectroscopic investigation of thermally induced structural evolution of a-C:H:Si film. *Appl. Surf. Sci.* **2020**, *541*, 148413. [[CrossRef](#)]
47. Åstrand, M.; Selinder, T.; Fietzke, F.; Klostermann, H. PVD-Al₂O₃-coated cemented carbide cutting tools. *Surf. Coat. Technol.* **2004**, *188–189*, 186–192. [[CrossRef](#)]
48. Podgursky, V.; Yashin, M.; Jõgiaas, T.; Viljus, M.; Alamgir, A.; Danilson, M.; Bogatov, A. high temperature tribological properties of Al₂O₃/NCD films investigated under ambient air conditions. *Coatings* **2020**, *10*, 175. [[CrossRef](#)]
49. Alamgir, A.; Yashin, M.; Bogatov, A.; Viljus, M.; Traksmäa, R.; Sondor, J.; Lümekemann, A.; Sergejev, F.; Podgursky, V. High-temperature tribological performance of hard multilayer TiN-AlTiN/nACo-CrN/AlCrN-AlCrO-AlTiCrN coating deposited on WC-Co Substrate. *Coatings* **2020**, *10*, 909. [[CrossRef](#)]
50. Mangolini, F.; Hilbert, J.; McClimon, J.B.; Lukes, J.R.; Carpick, R.W. Thermally induced structural evolution of silicon- and oxygen-containing hydrogenated amorphous carbon: A combined spectroscopic and molecular dynamics simulation investigation. *Langmuir* **2018**, *34*, 2989–2995. [[CrossRef](#)] [[PubMed](#)]
51. Scharf, T.W.; Ott, R.D.; Yang, D.; Barnard, J.A. Structural and tribological characterization of protective amorphous diamond-like carbon and amorphous CN_x overcoats for next generation hard disks. *J. Appl. Phys.* **1999**, *85*, 3142–3154. [[CrossRef](#)]
52. XPS Interpretation of Silicon. Available online: <https://xpssimplified.com/elements/silicon.php> (accessed on 1 April 2021).
53. Pu, J.-C.; Wang, S.-F.; Sung, J.C. High-temperature oxidation behavior of nanocrystalline diamond films. *J. Alloy. Compd.* **2010**, *489*, 638–644. [[CrossRef](#)]
54. Kudin, K.N.; Ozbas, B.; Schniepp, H.C.; Prud'Homme, R.K.; Aksay, I.A.; Car, R. Raman spectra of graphite oxide and functionalized graphene sheets. *Nano Lett.* **2008**, *8*, 36–41. [[CrossRef](#)] [[PubMed](#)]
55. Doremus, R.H. Diffusion in alumina. *J. Appl. Phys.* **2006**, *100*, 101301. [[CrossRef](#)]